In situ study of phase transformation at elevated temperature and correlated mechanical degradation of nitrogen implanted Ti-6Al-4V alloys

F. Berberich[1], W. Matz[1,2], E. Richter[1], N. Schell[2]
[1]Institute of Ion Beam Physics and Materials Research, [2] Project-Group ESRF-Beamline
Forschungszentrum Rossendorf, P.O. Box 51 01 19, 01314 Dresden, Germany

1. Introduction

Ti-6Al-4V (wt.%) is one of the mostly used titanium alloys. Compared to pure titanium it has a similar low density but favourable physical and mechanical properties. The higher tensile strength, hardness and proof stress, the lower elongation or the good corrosion resistance make it interesting for technical applications ranging from construction materials (aeronautics, submarines) [1] to medical implant materials [2, 3]. However, the untreated alloy surface often has nonsufficient tribological properties [4, 5]. A poor wear behaviour is not acceptable for a rotating part (e.g. in a turbine) or for a medical implant material (not only because of the potential toxicity).

It was shown that a nitrogen implantation treatment can improve the surface hardness and/or tribological properties [6, 7, 8]. This ion treatment works well for medical applications like knee and hip-joint prostheses. However, for the application in aerospace industry, which accounts for more than 80% of Ti-6Al-4V usage [9], a good performance at higher temperature is also desired. Therefore, it is important to understand the mechanisms of hardening and the stability of the improved surface quality at higher temperatures.

Samples treated with ion beam implantation (IBI) and plasma immersion ion implantation (PIII) were compared. IBI allows to deposit nitrogen in wide range of depth depending on the implantation energy. However, this method works only for plane surfaces and takes a long implantation time, whereas the PIII method seems more suitable for industrial applications because of lower costs, the shorter implantation times and its easier handling. For work pieces with irregular surface no sample manipulation is necessary [10].

To understand the structural changes in the nitrogen implanted layer near the surface of the Ti-6Al-4V alloy at higher temperatures, x-ray diffraction by grazing incidence technique (GIXRD) was performed at ROBL [11]. The use of a high-temperature chamber and synchrotron radiation allows *in situ* experiments in times comparable to technical annealing procedures.

2. Experimental

Samples from commercial polycrystalline Ti-6Al-4V alloys (wt.%) were cut from a rod to disc specimens of 25 mm diameter and 2 mm thickness. These specimens were grinded and finally polished with a colloidal silica polishing suspension.
A slight fibre texture of the material was determined from XRD pole figures. Therefore, the sample orientation was selected in a direction of practical no textural change. For all the X-ray experiments the same sample orientation was used in order to exclude texture influences.

The implantations were done at the Forschungszentrum Rossendorf. IBI was performed with a DANFYSIK 1090 Ion Implanter with fluences of 1, 3 and $6x10^{17}$ N^+/cm^2 at an energy of 20, 80 and 180 keV. Such implantation leads to a Gaussian nitrogen profile at a depth of 150 nm for 80 keV or 300nm for 180 keV. The temperature at the sample surface measured by a thermocouple was below 200°C.

For the PII implantation the plasma was produced by an electron cyclotron resonance source (ECR) in a UHV chamber. The nitrogen gas (N_2^+) had a pressure of 0.2 Pa, the voltage was 40 kV, the power 350 W, the frequency 400 Hz and the pulse duration 5 µs. Under these conditions the sample temperature was also maintained below 200°C in order to avoid direct nitrogen diffusion into the alloy. The implantation time respectively the number of pulses was adopted to have a fluence of 1.7 x 10^{17} N/cm^2.

After the implantation the microhardness depth profiles were recorded using an ultramicrohardness tester from Shimadzu. The hardness was recorded with a Vickers indenter at a maximum load of 5 mN, 10 mN and 50 mN, respectively, for the as received, implanted and annealed samples.

The *in situ* x-ray diffraction experiments were performed at ROBL at the wavelength of 0.154 nm. Grazing incidence technique was applied. By varying the angle of incidence from 0.5° to 4° depth dependent structural information from 0.1 to 1 µm below the surface can be obtained assuming an average density of 4.43 g/cm^3 for Ti-6Al-4V.

3. Implantation and its effect on hardness

Fig. 1 shows the relative hardness-depth functions for a maximum load of 5 mN, normalised to the unimplanted sample for the PIII and the IBI at different annealing temperatures. Two different types of behaviour are observed.

For PII, the as implanted sample and those with low annealing temperatures have typical profiles of a near surface hardening effect, where the relative hardness value tends to 1 with increasing penetration depth. The maximum of the hardness increase (factor 1.4) is

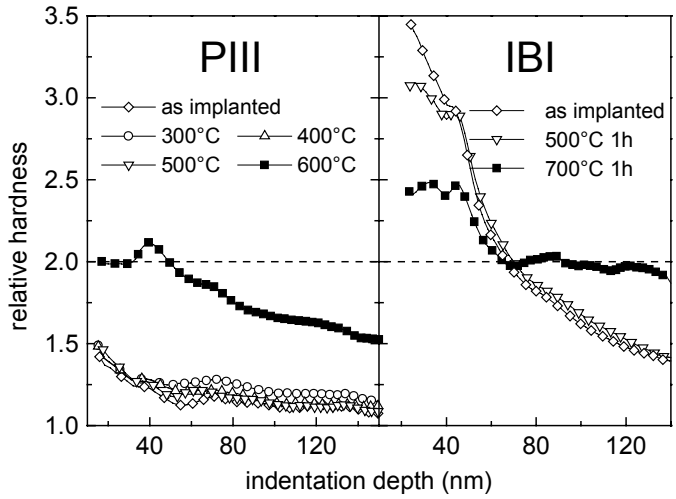

Fig. 1:
Relative hardness as function of indentation depth for PII and IBI implanted Ti-6Al-4V at different annealing temperatures.

found immediately below the surface. In contrast, the hardness-depth function for the sample annealed at 600°C shows first an increase until a relative hardness of about 2.1. Then in the deeper regions the hardness rests on a high level of approximately 1.5 times the value of the virgin material.

In comparison IBI samples for an implantation energy of 80 keV and a fluence of 6x10^{17} N$^+$/cm^2 show a completely different hardness behaviour with annealing temperature. Here, the N implantation increases the surface hardness up to 350% and the hardness depth function shows an exponential decay nearly to the original value (120%). After annealing at 500°C the surface hardness decreases only slightly to 86% and in the deeper regions no difference compared to the as-implanted sample is observed. However, after annealing at 700°C the surface hardness decreases to 70% of the as-implanted value, whereas it increases in deeper regions compared to all other treatments of the alloy. At depth of between 70 and 140 nm the relative hardness reaches about 200% of the virgin material.

4. Structural characterisation with synchrotron light

4.1 Phase transformation with increasing temperature

In order to characterise the structural changes in the N implanted samples at elevated temperature, which should be the reason of the changed hardness reported above, *in situ* XRD experiments were performed. PII and IB implanted Ti-6Al-4V samples were used. For both implantation methods the same structural characteristics are observed. The scanning time for each diffraction pattern was 30 min. So the duration of the *in situ* experiment corresponds to the typical annealing time used for such alloys. When comparing the diffraction pattern measured at incidence angles of 1° and 4°, respectively, the formation of the TiN phase is seen much more clearly at the measurement sensitive to the surface layer. Fig. 2 depicts the spectra at the angle of incidence of 1°.

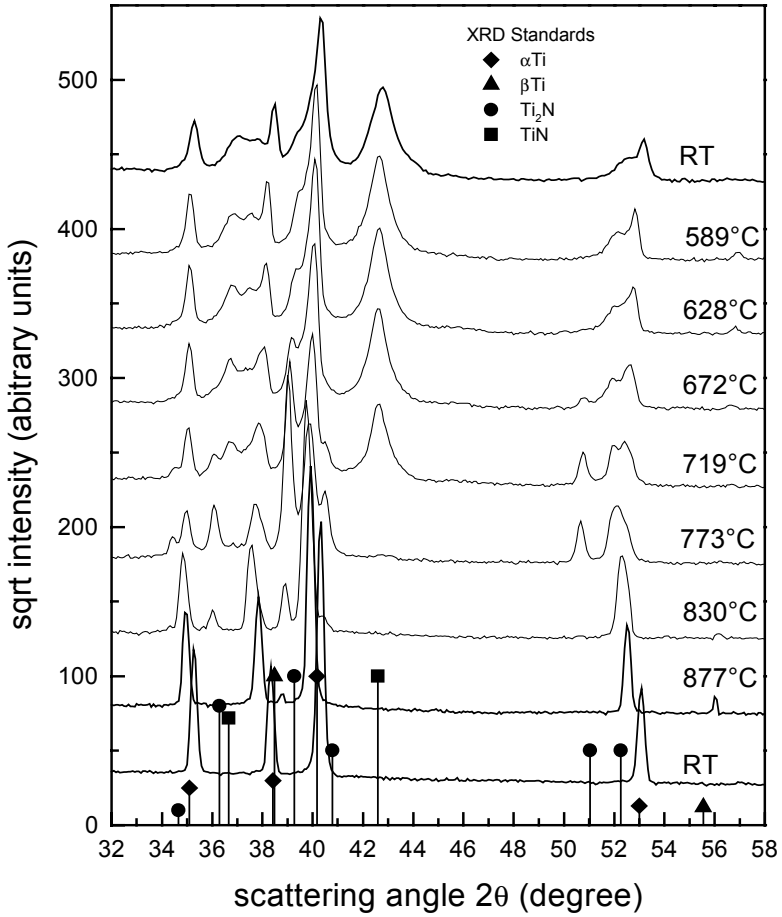

Fig. 2: Synchrotron radiation XRD pattern recorded at the angle of incidence of 1° and a wavelength of 0.154 nm during *in situ* annealing. The Ti-6Al-4V alloy was nitrogen implanted using IBI method at 80 keV with a fluence of $6x10^{17}$ N^+/cm^2. The Bragg peak positions of the phases as taken from the data base are indicated.

The pattern of the as-implanted alloy (corresponding to the upper RT curve in Fig. 2) consists of the Bragg peaks from both Ti phases (α + β) and cubic TiN formed by implantation. The hexagonal α-Ti phase is the dominating one in this alloy. The lattice constant of TiN was measured to be *a* = 0.4207 nm which is -0.8% different from the value for the stoichiometric phase [12]. It may be the indication for a nitrogen deficit or compressive stress in the grains, which can not be decided from the available data. The TiN peaks are very broad, indicating a small crystallite size of only about 6-8 nm as calculated with the Scherrer formula.

Up to 500°C the pattern remains unchanged and with further increasing temperature the intensity of the TiN peaks decreases. This can be most clearly observed for the (200)TiN reflection at a scattering angle of 42.6° in Fig 2. The onset of Ti_2N formation is observed at temperatures between 628° and 672°C. At the temperature of 773°C the Ti_2N peaks are

developed very clearly. These peaks have a similar width as the former TiN peaks, indicating Ti_2N crystallites with average sizes of about 10 nm.
From the development of the integrated intensities for TiN and Ti_2N as function of temperature it can be seen that this phase transformation is a continuous process. Additional *in situ* experiments have shown that at a fixed temperature of 680°C the same result is obtained, but the process takes more time, the lower the temperature is.
With further increasing temperature the Ti_2N phase dissolves also. At 773°C the corresponding Bragg reflection are very clearly developed but at the next temperature step no Ti_2N phase is seen in the diffraction pattern. At 877°C the cubic high temperature phase β-Ti is detected but is not quenched during the slow cooling process after the experiment.

Another structural effect is the change in the lattice parameters in both the α-Ti and β-Ti phases, which is not conform with thermal expansion [13]. Especially, the lattice expansion of the β-Ti phase of 2% over a temperature range of 200 K is remarkable. It is known, that V in Ti reduces the cubic lattice parameter significantly [14]. From the behaviour one may conclude that the annealing is connected with a reduction of the V-content in the β-Ti.

The PIII treated material shows essentially the same behaviour [15]. At 500°C the pattern consists of the Bragg peaks from both Ti phases (α + β) and TiN formed by implantation. The lattice constant of TiN was estimated to be *a* = 0.4217 nm which is -0.7% different from the value for the stoichiometric phase [12]. The TiN peaks are again very broad, and the calculated crystallite size is with 10 nm a little bit higher than for the IBI case. With increasing temperature the intensity of the TiN peaks decreases. At 750°C however, a new peak comes up at a slightly lower Bragg angle than the TiN peak observed so far. It remains in the pattern after the annealing process when cooling the sample to room temperature. In isothermal time dependent experiments it was found, that this peak does not arise from a peak shift, but is growing only after the original TiN peak disappeared. The two other peaks belonging to the pattern of a cubic phase are also observed but with low intensity. The room temperature lattice parameter of the new phase TiN* arising after annealing at 750°C is slightly different and amounts to a = 0.428 nm.

The onset of Ti_2N formation is observed at temperatures between 600 and 650°C. At the final temperature of 750°C, as well as at the room temperature measurement after the annealing process, the Ti_2N peaks are much sharper than the former TiN peaks, indicating well developed crystallites of Ti_2N with mean sizes of 35-40 nm.

4.2 Depth resolved measurements

With variation of α_i, the incidence angle, the average penetration depth of the x-ray and hence the near surface region where phases are detected can be changed. Fig. 3 depicts two depth profiles recorded from a PII implanted Ti-6Al-4V sample. The profile of the as implanted sample shows all Bragg peaks in the range from 37 to 44 degrees.

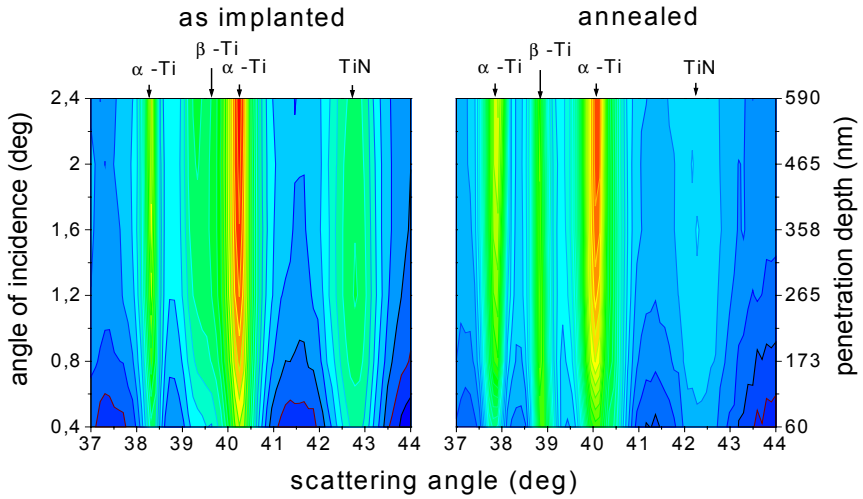

Fig. 3:
Depth profile of a PIII treated (40 keV / $1.7x10^{17}$ N^+/cm^2) Ti-6Al-4V alloy in the as implanted state and after annealing at 680°C for 1h.

The maximum of the TiN peak lies at an incidence angle of about 1.2 degree with corresponding average penetration depth of 270 nm. As this sample was PII implanted it is clear that the formation of TiN took place in the very surface region. At higher incidence angles only the reflections from the bulk increase in intensity. The high depth limit of the phase formation is difficult to determine because of accumulative nature of the scattering, so a scattering signal from the surface will be present at all higher α_i. Nevertheless some changes can be observed. The annealed sample shows a decreased intensity of the TiN peak and the maximum shifted towards higher depth. This is an obvious hint to a starting TiN dissolution and diffusion process. This result corresponds well with the changes in the hardness depth profiles after annealing. Another obvious change could be seen at the β-Ti Bragg reflection. In the annealed state it can be easily separated from the much more intense α-Ti reflection. This shows the expansion of the β-Ti phase mentioned above.

4.3 Activation energies

The annealing experiments with nitrogen implanted Ti-6Al-4V showed phase transformation from TiN to Ti_2N. In order to describe the temperature stability of TiN more quantitatively the activation energies for the dissolution of the TiN crystallites were determined. The kinetics of the dissolution process of the TiN phase was studied by recording the (200) Bragg peak during isothermal experiments at three different temperatures. The appropriate temperatures were estimated from the previously performed temperature scans. Some experiments were done at different incidence angles to compare the process in different depth but no significant changes were observed.
All measured peaks were fitted with Gaussian curves. Neglecting texture, the integrated intensity of the Bragg peak is proportional to the amount of crystallites of the phase of interest. With the data taken at three different temperatures it is possible to calculate the actual reaction velocities. From reaction velocities at different temperatures the activation energy is deduced by an Arrhenius plot.

Tab.1 gives an overview of the measured activation energies for the dissolution of TiN. For TiN an activation energy of (198 ± 14) kJ/mol is found for the temperature range 600°C - 800°C. The literature value [16] is given with 210 kJ/mol for a temperature range of 1300°C - 1670°C. For a comparison with the literature data one has to take into consideration that the activation energy is a temperature dependent value. So it seems that the values determined by XRD are realistic. The differences between the implantation modes obviously result from the different damage profile associated with implantation. The low energy implantations (IBI 20 keV; PIII 40 keV) produce TiN very near to the surface where also the main damage is located. Also implantation at 180 keV induces more damage and the TiN dissolution may be masked partially by damage recovery. The value for 80 keV IBI, which corresponds well with thermodynamic data, indicates that the Ti-6Al-4V matrix obviously has no significant influence on the stability of TiN.

Implantation method	Energy (keV)	Fluence (10^{17} N^+/cm^2)	Activation energy (kJ/mol)	
			measured	Ref. [16]
IBI	80	6.0	198±14	210 @ 1300°C
IBI	20	1.5	291±55	
IBI	180	6.0	277±17	
PII	40/20	1.7	328±68	

Tab. 1:
Activation energies for TiN calculated from the dissolution of TiN in Ti-6Al-4V. Two different ion implantation methods, beamline (IBI) and plasma ion immersion (PIII), are represented. Values for the IBI at different implantation energies and fluences.

5. Summary

Ti-6Al-4V alloy was implanted with nitrogen in order to enhance surface hardness. Two different implantation techniques (beamline and plasma immersion) were applied. The effects and mechanisms seem to be independent on the implantation method. Only the absolute values of changes differ. The hardness increase is correlated with the formation of TiN crystallites (size 6 to 10 nm) just below the surface. The nitrogen concentration is not sufficient to form a layer. Annealing partially destroys the additional surface hardening achieved by ion implantation at 600 to 700°C.

The structural changes in N implanted Ti-6Al-4V alloys were investigated with *in situ* XRD experiments. It was shown, that the phase transformation TiN to Ti_2N is the main process. It is a continuous process and connected with nitrogen diffusion at higher temperatures. The formation of TiN is located around the projected implantation range while the formation of Ti_2N as the higher temperature phase occurs also in deeper region as consequence of nitrogen diffusion. The existence of Ti_2N in the alloy is responsible for the remaining hardness after annealing. From crystallite size, total nitrogen concentration and the similar effect of TiN and Ti_2N it was concluded that dispersion hardening is the relevant mechanism.

The determination of the activation energies of the dissolution of the formed TiN crystallites gives a hint at the stability of TiN in Ti-6Al-4V and allow to estimate a temperature limit where the phase remains stable. In addition to the structural investigation also elastic recoil detection analysis was applied which supports the onset of a diffusion process after a threshold temperature.

References

[1] M. Peters, J. Kumpfert, C. Leyens in: Titan und Titanlegierungen, ed. M. Peters, J. Kumpfert, C. Leyens; DGM Informationsgesellschaft Verlag, Oberursel, 1996, p. 187-203
[2] R. van Noort, J. Mater. Sci., **22** (1987) 3801-3811.
[3] P. Sioshansi, Nuclear Instr. and Methods, **B 18-20** (1987) 204-208.
[4] S.M. Johns, T. Bell, M. Samandi and G.A. Collins, Surf. Coatings Technol., **85** (1996), 7-14.
[5] I.C. Clarke, H.A. McKellop, P. McGuire, R. Okuda and A. Sarmiento, in: Titanium in Surgical Implants, ASTM STP 766, 1983, pp. 136-147.
[6] K.-T. Rie, T. Stucky, R.A. Silva, E. Leitão, K. Bordji, J.-Y. Jouzeau and D. Mainard, Surf. Coatings Technol., **74-75** (1995) 973-980.
[7] T.M. Muraleedharan, E.I. Meletis, Thin Solid Films, **221** (1992) 104-113.
[8] A. Loinanz, M. Rinner, F. Alonso, J.I. Oñate and W. Ensinger, Surf. Coatings Technol., **103-104** (1998), 262-267.
[9] R. Boyer, G. Welsch and E. Collings, Materials Properties Handbook: Titanium Alloys, ASM Ohio 1994, 483 ff.
[10] W. Matz, N. Schell, G. Bernhard, F. Prokert, T. Reich, J. Claußner et al., J. Synchrotron Rad., **6** (1999) 1076-1085.
[11] W. Möller, E. Richter, Galvanotechnik, **89** (1998) 858.
[12] Powder diffraction file PDF-2, No. 38-1420; ICDD, Newton Square, PA 19073-3273, USA
[13] F. Berberich, W. Matz, E. Richter, N. Schell, U. Kreißig, W. Möller, Surf. Coatings Technol., **128-129** (2000), 418-422.
[14] U. Zwicker, Titan und Titanlegierungen, Springer-Verlag, Berlin, 1974, p. 68.
[15] F. Berberich, W. Matz, U. Kreissig, E. Richter, N. Schell, W. Möller, Appl. Surf. Sci. (2001) in press
[16] F.W. Wood, O.G. Paasche, Thin Solid Films, **40** (1977) 133-137.